



ELSEVIER

Contents lists available at ScienceDirect

Journal of Magnetism and Magnetic Materials

journal homepage: www.elsevier.com/locate/jmmm

Plane-wise sensitivity based inhomogeneous excitation fields for magnetorelaxometry imaging of magnetic nanoparticles

Daniel Baumgarten^{a,b,*}, Friedemann Braune^a, Eko Supriyanto^b, Jens Hauelsen^a^a Institute of Biomedical Engineering and Informatics, Technische Universität Ilmenau, 98693 Ilmenau, Germany^b IJN-UTM Cardiovascular Engineering Centre, Universiti Teknologi Malaysia, 81310 UTM Skudai, Johor Bahru, Malaysia

ARTICLE INFO

Article history:

Received 30 June 2014

Received in revised form

21 August 2014

Accepted 2 September 2014

Available online 10 September 2014

Keywords:

Magnetic nanoparticle

Magnetorelaxometry

Imaging

Inhomogeneous excitation

Spatial sensitivity

ABSTRACT

Promising biomedical applications of magnetic nanoparticles share the need for a quantitative knowledge of their in vivo distribution. From multichannel magnetorelaxometry measurements with sequential activation of inhomogeneous excitation fields, the distribution can be quantitatively determined. In first studies, single excitation coils were consecutively activated. We aim at further advancing this imaging technology by suitable activation patterns involving multiple excitation coils. In this work, we propose the estimation of these patterns based on the spatial sensitivity in order to reduce the number of required measurements. The sensitivity of a voxel carrying magnetic nanoparticles is determined by its position relative to the sensors and the excitation field. Whereas the position is fixed within a given setup, the excitation is controlled by the currents in the coils. The currents required for a defined target sensitivity are estimated by solving an inverse problem. In our work, two target sensitivity paradigms are presented: (a) plane-wise activation, where only one plane with high sensitivities is sought and moved through the source space and (b) plane-wise non-activation, where all voxels except for one plane should receive high sensitivity. Our approach is investigated in simulation studies using a setup with a cubic region of interest and a planar sensor array. The imaging quality of both activation paradigms is evaluated. Our results demonstrate the principal applicability of this spatial sensitivity based approach for defining inhomogeneous activation patterns. The obtained patterns allow for a similar imaging quality using a lower number of activation sequences compared to the conventional single coil activation.

© 2014 Elsevier B.V. All rights reserved.

1. Introduction

Magnetic nanoparticles offer a large variety of promising biomedical applications, among them magnetic drug targeting [1] and magnetic hyperthermia [2]. All these applications share the need for a quantitative and precise detection of the particles with respect to monitoring application safety and efficiency. Magnetorelaxometry (MRX) using superconducting quantum interference devices (SQUID) sensors is a highly sensitive and versatile technique for the detection and characterization of the particles [3]. From multichannel MRX measurements, the distribution of magnetic nanoparticles can be quantitatively determined [4,5]. In first simulations and experiments, homogeneous activation fields arising from exciting a Helmholtz coil pair were employed [6,7]. On the other hand, inhomogeneous magnetization fields can be obtained through the use of excitation coil arrays. The sequential activation of

distinct inhomogeneous fields and the combination of the consecutive measurement results considerably enhance the imaging quality compared to homogeneous activation of the particles [8,9]. This idea was experimentally implemented with consecutive single coil activation, revealing promising imaging results [10]. However, the consecutive activation of single coils leads to a high number of required measurements resulting in extended measurement times.

The primary objective of all these developments is the application of inhomogeneous magnetorelaxometry imaging in pre-clinical research with small animals, e.g. the spatially resolved quantification of nanoparticle accumulations during magnetic drug targeting applications [11]. For this purpose, we aim at further advancing this imaging technology by finding suitable activation patterns involving multiple excitation coils. In this respect, the number of required measurements should be reduced without impairing the imaging quality. Creveceour et al. presented a first approach for defining these patterns by determining coil currents that generate a preferably homogeneous spatial sensitivity within the source space [12]. In another simulation study, the coil arrays were sequentially activated based on previous reconstructions of particle distribution [13].

* Corresponding author at: Institute of Biomedical Engineering and Informatics, Technische Universität Ilmenau, 98693 Ilmenau, Germany. Tel.: +49 3677 69 1309.
E-mail address: daniel.baumgarten@tu-ilmenau.de (D. Baumgarten).

In this paper, we present approaches for defining the excitation patterns based on the spatial sensitivity in the source space independent from the actual measurement object. More specifically, these patterns consecutively sensitize specific sub-volumes of the source space. Two paradigms seeking different sub-volumes are described and compared in simulation studies.

2. Methods

2.1. Forward and inverse modeling

Dividing the source space of an MRX experiment into N_v volume elements, the contribution of one voxel at location \vec{r}_k containing an amount of n_k particles with the magnetic susceptibility χ to the magnetic flux density B in the sensor location \vec{r}_s can be formulated as

$$B(\vec{r}_s) = \frac{\mu_0}{4\pi} \vec{d}_s \sum_{k=0}^{N_v} \left[\left(\frac{3\vec{r}_s \vec{r}_k}{|\vec{r}_s|^5} - \frac{1}{|\vec{r}_s|^3} \right) \cdot \vec{H}(\vec{r}_k) \cdot \chi \cdot n_k \right] \quad (1)$$

with $\vec{r} = \vec{r}_s - \vec{r}_k$ and \vec{d}_s being the normal vector of the SQUID's flux pickup loop. $\vec{H}(\vec{r}_k)$ is the magnetization field in this voxel, generated by the excitation coils. Summarizing these equations for all voxels and sensors leads to

$$\vec{b}_0 = \mathbf{L}_0 \cdot \vec{n} \quad (2)$$

with the vectors \vec{b}_0 and \vec{n} containing the relaxation amplitudes in the sensors and the particle concentrations in the voxels, respectively. \mathbf{L}_0 is the system matrix with the dimension $N_s \times N_v$ (N_s -number of sensors). Combining multiple measurements with different excitation fields results in a concatenated measurement vector \vec{b} of length $N_m \cdot N_s$ (N_m -number of measurements) and a system matrix \mathbf{L} that is composed of the system matrices of the single measurements and therefore has the dimensions $N_m \cdot N_s \times N_v$ [9]:

$$\vec{b} = \mathbf{L} \cdot \vec{n} \quad (3)$$

The amount of particles in the voxels can be estimated by minimizing the L_2 norm of the difference between this forward model and the measured relaxation amplitudes \vec{b}_{meas} :

$$\vec{n}_{est} = \underset{\vec{n}}{\operatorname{argmin}} \|\mathbf{L} \cdot \vec{n} - \vec{b}_{meas}\| \quad (4)$$

The problem is solved using the Moore–Penrose pseudo-inverse and Truncated Singular Value Decomposition regularization [6].

2.2. Spatial sensitivity

The impact of the k th voxel on the sensor system is given by the spatial sensitivity S_k :

$$S_k = \sum_{s=1}^{N_s} \|\mathbf{L}_{sk}\| \quad (5)$$

In this respect, the elements of the system matrix \mathbf{L} and therewith the sensitivity are influenced by two main contributions, i.e. the positions of voxels, sensors and excitation coils as well as the excitation field in the respective voxel. The sensitivity decreases for larger distances of the voxel to the sensors and with smaller excitation fields. Whereas the position is fixed within a given setup, the excitation field in each voxel can be controlled by the currents in the excitation coils. The N_v -dimensional vector \vec{S} containing the sensitivities in the voxels can be computed from the activation currents vector \vec{I}_c with the dimension N_c (N_c -number of coils) by an interaction matrix \mathbf{A} ($N_v \times N_c$):

$$\vec{S} = \mathbf{A} \cdot \vec{I}_c \quad (6)$$

In order to specifically excite* a sub-region of the source space, a target sensitivity pattern \vec{S}^* is defined [12]. Solving an overdetermined inverse problem, the coil currents generating the target sensitivity can be approximated using the Moore–Penrose pseudo-inverse \mathbf{A}^+ of \mathbf{A} :

$$\vec{I}_c^* = \mathbf{A}^+ \cdot \vec{S}^* \quad (7)$$

2.3. Excitation patterns

The method described above is valid for different target sensitivity patterns. In this paper, two paradigms for defining the target sensitivity are proposed. The *plane-wise activation paradigm* seeks a sensitivity $S_k^* = 1$ for all voxels within one plane of the source space (cf. Fig. 1), whereas all other voxels should receive a minimal sensitivity of $S_k^* = 0$. The excitation currents estimated for this target sensitivity are employed in one measurement. For the subsequent measurement, the next voxel plane is selected to receive high sensitivity. In this manner, the active plane is consecutively moved through the complete source space in all three orientations, defining one current pattern for each target sensitivity. Thus, the total number of measurements equals the number of planes in the source space.

In the *plane-wise non-activation paradigm*, all voxels except for one plane should receive a sensitivity of $S_k^* = 1$ in each measurement sample. For the voxels in the non-active plane, a sensitivity of $S_k^* = 0$ is sought. As in the first paradigm, this plane is moved through the source space in all three orientations, leading to the same number of measurements.

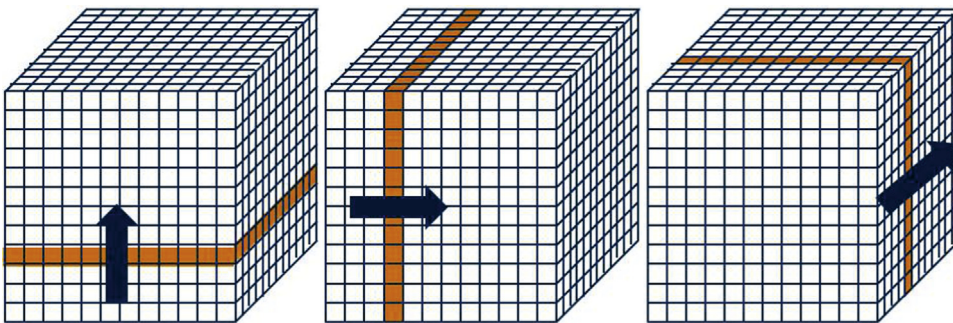


Fig. 1. Target sensitivities following the plane-wise activity paradigm: one active voxel plane in three orientations is consecutively moved through the source space.

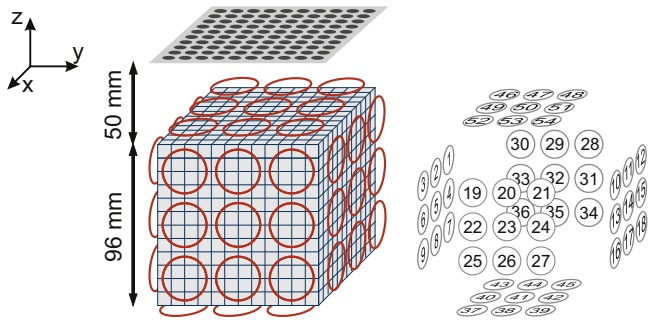


Fig. 2. Schematic representation of the simulation setup with the excitation coils positioned in 6 planes around the source region containing $12 \times 12 \times 12$ voxels and one plane of sensors above the sources (left) as well as indices of the excitation coils (right).

2.4. Simulation setup

The paradigms proposed above are investigated in simulation studies involving a simplified geometric setup. This setup represents a possible realistic implementation of sequential inhomogeneous activation. It comprises 54 excitation coils with a uniform diameter $d=30$ mm positioned in all 6 planes around the region of interest with a distance of 5 mm (cf. Fig. 2). In each plane, 9 coils are arranged in a regular grid with distances of 35 mm between the coil centers, respectively.

A sensor system with a total of 100 magnetic sensors placed on a regular grid in a distance of 50 mm above the source space is considered. The sensors ($d=5$ mm) are oriented with their normal vectors in the z -direction. The source space is divided into $12 \times 12 \times 12$ cubic volume elements with an edge length of 8 mm, located central below the sensor system.

Two different distributions of magnetic nanoparticles are simulated. One distribution emulates the Shepp–Logan phantom with three different particle concentrations in a $12 \times 12 \times 12$ voxel volume. Fig. 4a visualizes the voxels of the yz -planes of the three-dimensional distribution plotted side by side; the x -position of each plane is indicated above. Furthermore, a checkerboard phantom is employed (cf. Fig. 6a). Likewise, it is composed of $12 \times 12 \times 12$ volume elements. These voxels alternately contain high and very low particle concentrations.

3. Results

3.1. Estimated activation currents and achieved sensitivities

The excitation currents estimated for the described setup and plane-wise activation are illustrated in Fig. 3 (left column, coil indices corresponding to Fig. 2). Presented are selected samples, aiming at a bottom, central and top xy -plane (a–c) as well as a left and central xz -plane (d, e), respectively. With respect to the symmetry of the simulated setup, the results are analog for a right xz -plane. In the vertical planes (coils 1–36), the coils near the target planes yield higher currents, predominantly in one direction. The coils in the grid below the source space (coils 37–45) yield high currents for all target sensitivity patterns to compensate for the large distance to the sensors. However, it can be seen that the currents within this plane have reverse orientations, partly canceling out each other. The currents assigned to the coils above the source space (coils 46–54) are small, even when targeting the top plane.

The right column of Fig. 3 visualizes the central yz -plane ($x=44$ mm) of the sensitivity patterns realized with the corresponding currents. In all cases, voxels with high sensitivity are

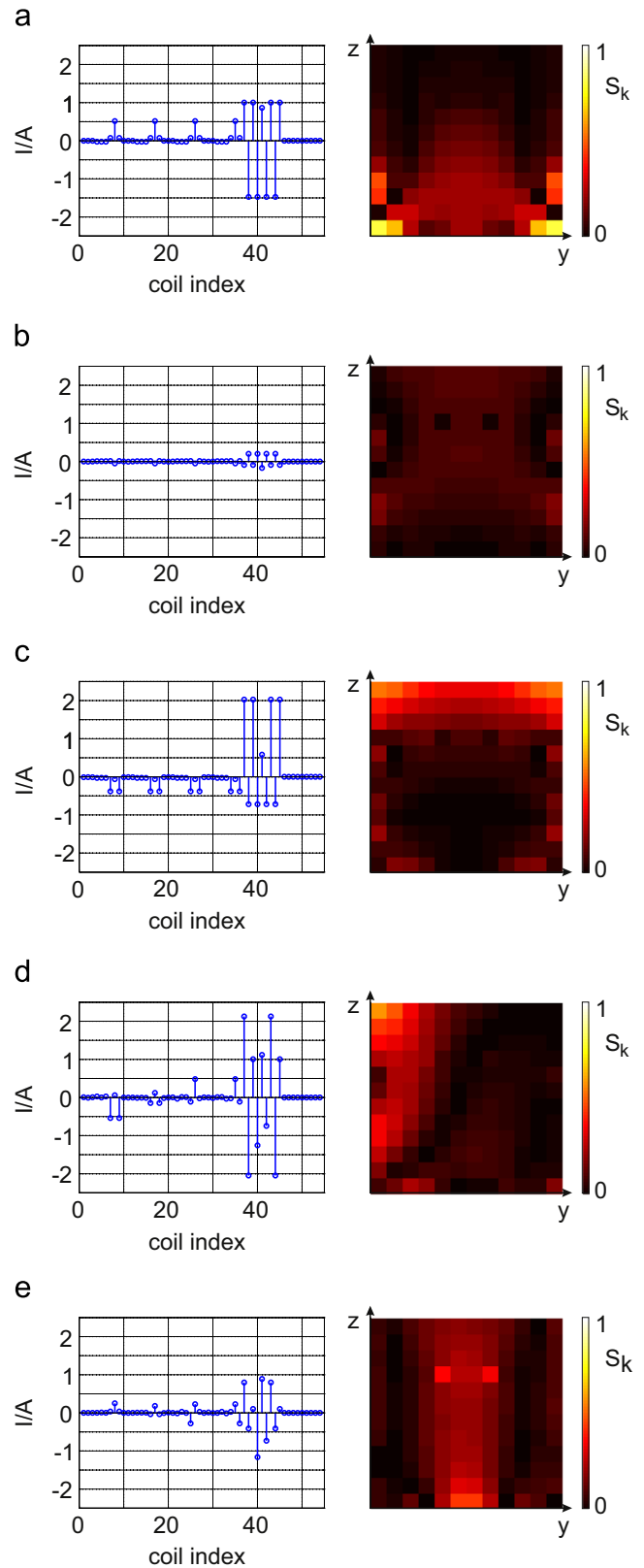


Fig. 3. Left: estimated currents in the excitation coils (indices corresponding to Fig. 2); right: respective sensitivity patterns in the central yz -plane ($x=44$ mm) of the source space for a bottom, central and top xy -plane (a–c; samples 1, 6, 12) as well as a left and central xz -plane (d, e; samples 25, 30). (a) $s=1$, (b) $s=6$, (c) $s=12$, (d) $s=25$ and (e) $s=30$.

visible near the activated coils, whereas other voxels within the target plane exhibit considerably lower sensitivity. Furthermore,

the sensitivity is generally blurred over more than one plane in all cases. Regarding these limitations, horizontal and vertical planes near the excitation coils can be sensitized well (a, c, d). A horizontal central plane is hard to focus (b), whereas the central vertical plane can be nicely addressed (e).

3.2. Imaging results

Fig. 4 visualizes reconstructed distributions of magnetic nanoparticles employing optimized activation currents following the two presented paradigms (Fig. 4b and c) as well as the conventionally employed consecutive activation of a single coil per measurement (Fig. 4d). In each subfigure, the yz -planes are displayed side by side with their x -coordinates corresponding to subfigure (a). The reconstruction result of the plane-wise activation paradigm involving 36 measurements (b) exhibits a correlation to the simulated source of $c=0.9971$. The result of plane-wise non-activation with the same number of measurements is displayed below ($c=0.9956$). Visual inspection yields similarly good imaging results for both paradigms, confirmed by the high correlation values. The outer shape of the phantom is ideally reconstructed with sharp contours. In both cases, minimal perturbations appear in the lower part of the distributions. Both reconstructions yield good agreement with the quantitative values of the simulated source (cf. Fig. 4a). In comparison, Fig. 4d illustrates the reconstructed particle distribution in the voxels when consecutively activating one single coil per measurement. This conventional approach leads to 54 measurements. The reconstruction exhibits a correlation to the simulated source of $c=0.9989$ and reveals no visible differences to the results of both plane-wise paradigms. In a further simulation, we reduced the number of target sensitivity patterns and therewith measurements from 36 to 12. As Fig. 5 illustrates, activating 12 planes yields a good reconstruction in the top planes close to the sensors, whereas in the lower part the boundaries and inner structures are disturbed compared to the results obtained from 36 measurements. In this respect, addressing the 12 xy -planes (subfigure a; $c=0.9625$) reveals similar visual results and correlation values as targeting 4 planes per orientation, i.e. 4 xy -, xz -, and yz -planes,

respectively (subfigure b; $c=0.9680$). Again, the concentration values could be quantitatively reconstructed.

In order to approach the limitations of our paradigms, we employed a checkerboard phantom containing the highest possible spatial frequencies in the simulated source space. The imaging result from simulations of this phantom employing the plane-wise activation paradigm is illustrated in Fig. 6b. Only small perturbations of the voxel pattern in the lower central part can be observed. Voxels with high concentrations are correctly reconstructed, whereas the distribution is smeared over the empty voxels in these perturbed areas. The small loss of imaging quality is substantiated by the high correlation value of $c=0.9907$ between the simulated and reconstructed distribution.

4. Discussion

Our work aims at finding optimal excitation currents in magnetorelaxometry imaging of magnetic nanoparticles. These currents should reduce the number of required measurements while preserving the imaging quality compared to the previously employed consecutive single coil activation. In this paper, we propose the determination of these currents based on target patterns of the spatial sensitivity in the source space. Two paradigms for defining the target sensitivity patterns are proposed: plane-wise activation and plane-wise non-activation. In contrast to approaches presented earlier [13], this methodology allows for the determination of appropriate excitation patterns prior to the actual measurement and independent from the measurement object. Since the evaluation and analysis of the measurement data is time-consuming in current systems, an adaptation of the excitation to the sample under investigation is challenging. On the other hand, homogeneous spatial sensitivity in the source space as proposed by Crevecoeur et al. [12] ensures that all parts of the volume of interest contribute to the signal in the sensors within one measurement. This approach poses restrictions in terms of the spatial resolution. Since all voxels contribute to the sensor signal within a single excitation pattern, spatial information is lost, particularly in the z -direction. The consecutive activation of

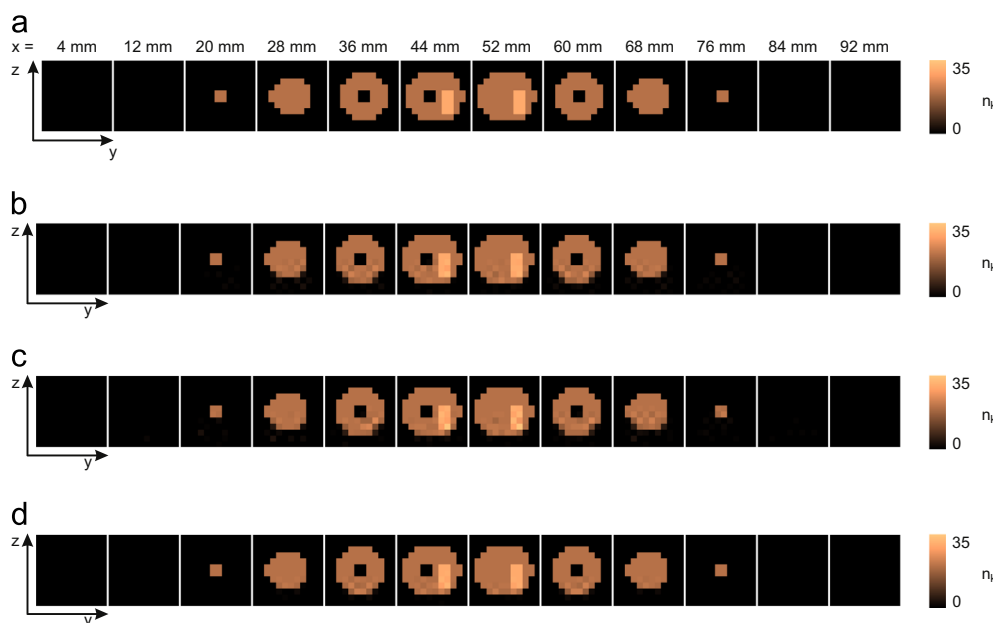


Fig. 4. Distribution of magnetic nanoparticles emulating a Shepp-Logan phantom (yz -planes, plotted side by side): simulated distribution (a) and reconstructed distributions following different activation paradigms (b–d). (a) Simulation particle distribution, (b) Imaging result employing plane-wise activation with all 36 planes ($c = 0.9971$), (c) imaging result employing plane-wise non-activation with all 36 planes ($c = 0.9956$) and (d) imaging result employing consecutively activated single coils (correlation: $c = 0.9989$).

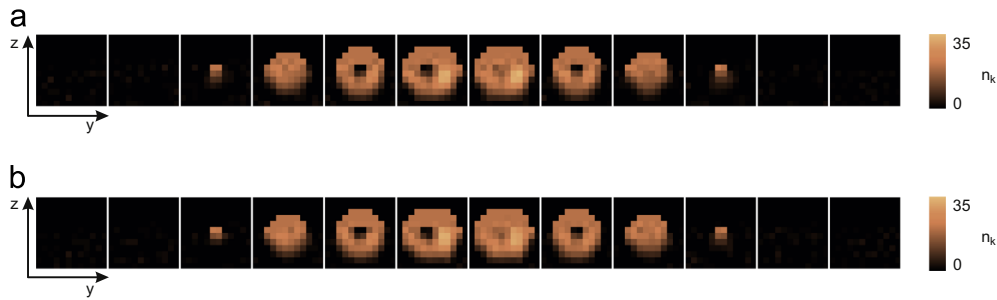


Fig. 5. Distributions of magnetic nanoparticles (xz -planes) reconstructed from simulations of the Shepp–Logan phantom following the plane-wise activation paradigm with reduced number of target planes. (a) 12 xy -planes ($c=0.9625$). (b) 12 planes (4 xy , 4 xz , 4 yz ; $c=0.9680$). (a) 12 xy -planes ($c = 0.9625$) and (b) 12 planes (4 xy , 4 xz , 4 yz ; $c = 0.9680$).

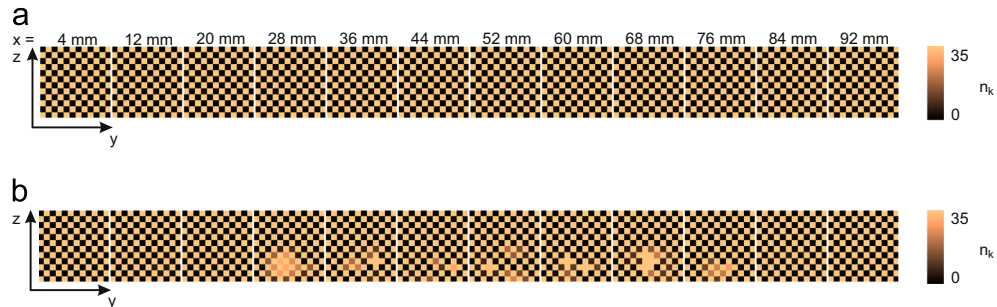


Fig. 6. Checkerboard phantom of magnetic nanoparticles (xz -planes) simulated (a) and reconstructed from these simulations following the plane-wise activation paradigm (b). (a) simulated distribution and (b) reconstructed distribution using plane-wise activation paradigm with all 36 planes ($c = 0.9907$).

sub-volumes as proposed in this paper enables a better discrimination between the signals from different voxels.

The excitation currents obtained with our approach allow for the activation of different sub-volumes. Due to the underlying physical principles, the magnetic field and therewith the sensitivity cannot be focused in the center of the source space. Therefore, only a low sensitivity can be achieved in horizontal central planes. However, since the sensitivity also depends on the distance to the sensors, vertical central volumes can be addressed. Another reason for the blurring of the sensitivity patterns over several planes is the application of a least squares approach for their estimation. The employment of different inverse methods or the introduction of constraints, e.g. to the current amplitudes, can lead to more focused sensitivity patterns. The sensor and excitation setup involved in the simulations of this paper represent a suitable combination for pre-clinical research with small animals. The spatial resolution of 8 mm^3 allows for the spatially resolved quantification of multiple nanoparticle accumulations. The employed Shepp–Logan phantom represents a realistic particle distribution. Our imaging results demonstrate that the variety of the sensitized sub-volumes is sufficient for this setup and spatial resolution. The three-dimensional particle distributions could be reconstructed using the sensitivity based approach. Both proposed paradigms, i.e. plane-wise activation and plane-wise non-activation, yield similar results. The Shepp–Logan phantom could be reconstructed with the same quality in terms of visual inspection and correlation compared to the consecutive single coil activation. The imaging results of the checkerboard phantom demonstrate the limitations of the proposed paradigms for high spatial frequencies, which rarely occur in real measurements.

Reducing the number of activated planes and therewith measurements impair the imaging quality. One might expect that in this respect, the activation of all xy -planes is favorable due to the dimension and orientation of the sensor plane. However, our results demonstrate that for the given setup, these reconstructions yield similar results compared to selecting 4 planes per orientation. One

possible reason is the higher number of central xy -planes involved in the measurements, which are more difficult to be activated.

5. Conclusion

The results presented in this paper demonstrate the principal applicability of the proposed approach and the two paradigms for defining inhomogeneous activation patterns in magnetorelaxometry imaging of magnetic nanoparticles. The obtained patterns allow for a comparable imaging quality with a considerably lower number of activation sequences compared to single coil activation. Therewith, a substantial reduction of the measurement time can be achieved, opening new options in experimental investigations. Thus, further investigations will be performed emulating more realistic measurement conditions in terms of setups, noise and applicable currents in the excitation coils. Moreover, we aim at further improving our approach by employing different inverse algorithms for determining the excitation currents as well as employing sophisticated target sensitivity patterns.

Acknowledgments

This work was supported by the German Research Foundation (DFG; Grant BA4858/1-1) and the German Federal Ministry of Education and Research (BMBF) as part of the Innoprofile Transfer project MAMUD (Grant O3IPT605X).

References

- [1] C. Alexiou, R. Tietze, E. Schreiber, R. Jurgons, H. Richter, L. Trahms, H. Rahn, S. Odenbach, S. Lyer, Cancer therapy with drug loaded magnetic nanoparticles –magnetic drug targeting, *J. Magn. Mater.* 323 (10) (2011) 1404–1407. <http://dx.doi.org/10.1016/j.jmmm.2010.11.059>.

- [2] R. Hiergeist, W. Andra, N. Buske, R. Hergt, I. Hilger, U. Richter, W. Kaiser, Application of magnetite ferrofluids for hyperthermia, *J. Magn. Magn. Mater.* 201 (1999) 420–422. [http://dx.doi.org/10.1016/S0304-8853\(99\)00145-6](http://dx.doi.org/10.1016/S0304-8853(99)00145-6).
- [3] F. Wiekhorst, U. Steinhoff, D. Eberbeck, L. Trahms, Magnetorelaxometry assisting biomedical applications of magnetic nanoparticles, *Pharm. Res.* 29 (5) (2012) 1189–1202. <http://dx.doi.org/10.1007/s11095-011-0630-3>.
- [4] F. Wiekhorst, C. Seliger, R. Jurgons, U. Steinhoff, D. Eberbeck, L. Trahms, C. Alexiou, Quantification of magnetic nanoparticles by magnetorelaxometry and comparison to histology after magnetic drug targeting, *J. Nanosci. Nanotechnol.* 6 (9–10) (2006) 3222–3225. <http://dx.doi.org/10.1166/jnn.2006.477>.
- [5] H. Richter, M. Kettering, F. Wiekhorst, U. Steinhoff, I. Hilger, L. Trahms, Magnetorelaxometry for localization and quantification of magnetic nanoparticles for thermal ablation studies, *Phys. Med. Biol.* 55 (3) (2010) 623–633. <http://dx.doi.org/10.1088/0031-9155/55/3/005>.
- [6] D. Baumgarten, M. Liehr, F. Wiekhorst, U. Steinhoff, P. Münster, P. Miethe, L. Trahms, J. Haueisen, Magnetic nanoparticle imaging by means of minimum norm estimates from remanence measurements, *Med. Biol. Eng. Comput.* 46 (12) (2008) 1177–1185. <http://dx.doi.org/10.1007/s11517-008-0404-1>.
- [7] D. Baumgarten, J. Haueisen, A spatio-temporal approach for the solution of the inverse problem in the reconstruction of magnetic nanoparticle distributions, *IEEE Trans. Magn.* 46 (8) (2010) 3496–3499. <http://dx.doi.org/10.1109/TMAG.2010.2043344>.
- [8] N. Sepúlveda, I. Thomas, J.P. Wikswo, Jr., Magnetic susceptibility tomography for three-dimensional imaging of diamagnetic and paramagnetic objects, *IEEE Trans. Magn.* 30(6) (1994) 5062–5069. <http://dx.doi.org/10.1109/20.334296>.
- [9] U. Steinhoff, F. Wiekhorst, D. Baumgarten, J. Haueisen, L. Trahms, Imaging of magnetic nanoparticles based on magnetorelaxometry with sequential activation of inhomogeneous magnetization fields, *Biomed. Tech.* 55 (2010) 22–25. <http://dx.doi.org/10.1515/BMT.2010.104>.
- [10] M. Liebl, U. Steinhoff, F. Wiekhorst, A. Coene, J. Haueisen, L. Trahms, Quantitative reconstruction of a magnetic nanoparticle distribution using a non-negativity constraint, *Biomed. Tech.* 58 (2013) 22–25. <http://dx.doi.org/10.1515/bmt-2013-4261>.
- [11] F. Wiekhorst, M. Liebl, U. Steinhoff, L. Trahms, S. Lyer, S. Dürr, C. Alexiou, Magnetorelaxometry for in vivo quantification of magnetic nanoparticle distributions after magnetic drug targeting in a rabbit carcinoma model, in: T.M. Buzug, J. Borgert (Eds.), *Springer Proceedings in Physics*, vol. 140, Springer, Berlin, Heidelberg, 2012, pp. 301–305. http://dx.doi.org/10.1007/978-3-642-24133-8_48.
- [12] G. Crevecoeur, D. Baumgarten, U. Steinhoff, J. Haueisen, L. Trahms, L. Dupre, Advancements in magnetic nanoparticle reconstruction using sequential activation of excitation coil arrays using magnetorelaxometry, *IEEE Trans. Magn.* 48 (4) (2012) 1313–1316. <http://dx.doi.org/10.1109/TMAG.2011.2173317>.
- [13] A. Coene, G. Crevecoeur, L. Dupre, Adaptive control of excitation coil arrays for targeted magnetic nanoparticle reconstruction using magnetorelaxometry, *IEEE Trans. Magn.* 48 (11) (2012) 2842–2845. <http://dx.doi.org/10.1109/TMAG.2012.2201706>.